Optical Spectra of Fe(II) Cytochrome *c* Interpreted Using Molecular Dynamics Simulations and Quantum Mechanical Calculations

Ninad V. Prabhu,† Sergio D. Dalosto,† Kim A. Sharp, W. W. Wright, and Jane M. Vanderkooi*

Johnson Research Foundation, Department of Biochemistry & Biophysics, School of Medicine, University of Pennsylvania, Philadelphia, Pennsylvania 19104

Received: November 14, 2001; In Final Form: February 14, 2002

Porphyrin electronic transitions in heme proteins provide a useful tool for probing the protein environment, since the surrounding protein affects the porphyrin π-electron cloud. Perturbations can arise from structural distortions of the porphyrin ring, from the internal electric field generated by charged and polar groups, or from axial ligation to the heme iron. In this work, cytochrome *c* in aqueous solution or in glasses of trehalose or glycerol/water was examined as a function of temperature to evaluate the effect of fluctuations on the heme. The amide I band of cytochrome *c* in trehalose remains constant over a wide temperature excursion, indicating that interactions between the protein and the matrix do not change with temperature. The width of the Q(0,0) optical transition measured at low temperature (i.e., <100 K) reflects the temperature at which the glass was formed, while the temperature profiles of the widths for the protein in different solvents and glasses are similar at high temperature. The results were interpreted in terms of contributions from solvent-coupled and solvent-uncoupled motions. Molecular dynamics simulations of cytochrome *c* in explicit solvent were performed to investigate the structural distortions in the protein, and semiempirical quantum mechanics (Zindo/S) was used to calculate the resultant changes in the spectroscopic transitions. A correlation between the calculated transition energies and the structural distortions in both the heme and the surrounding protein environment was observed and was invoked to characterize the origins of the temperature-dependent broadening of the electronic transitions seen in the visible spectra.

I. Introduction

Thermal motions of proteins are of considerable importance since even small changes in positions of the atoms of the prosthetic group or of the atoms near the active group can have a large influence on reactivity and physical parameters.

The subject of this paper is how disorder and motion of the protein atoms affects the spectral properties of the heme in ferrous cytochrome *c* (ferrous horse heart cytochrome *c*, cyt *c*). The optical spectral line of the heme Q(0,0) transition is monitored as a probe that is sensitive to solvent fluctuations and has relatively well understood properties that are approachable by computational methods. A feature of low-spin ferrous hemes is that an asymmetric protein environment may produce a split in the Q(0,0) absorption band.[1−4] Applications of computations to analyze hemoprotein spectra and the origin of the spectral splitting in cyt *c* are given in our papers with emphasis on axial ligation and the charges on the amino acids surrounding the heme.[5−7] Molecular dynamics has been used to study various structural and dynamical properties of members of the cyt *c* family. The relation of Debye−Waller factors from X-ray diffraction to atomic fluctuations,[8,9] the processes of dissipation of thermal energy within the protein atoms,[10,11] and the alteration in the electrostatic properties due to conformational changes[12−14] and fluctuations in the solvent-accessible surface areas[15] were the focus of some studies. In one case, fluctuations of the protein amino acids were examined and it was concluded that varying positions of charged groups were sufficiently large to produce spectral broadening.[16] It is well recognized that heme distortions change the spectra, but heretofore the dynamical features of the protein that result in distortions of the heme and a dynamically changing local electric field around the heme have not been both examined. Nor have the spectra been calculated to show the effect of the fluctuations.

In general, thermal perturbations can produce changes in the heme in the following ways: (1) structural distortions of the porphyrin ring, (2) axial ligation to the heme iron by one or more amino acid residues, or (3) the internal electric field generated by neighboring charged and polar groups. These three effects interact with each other in a complex way,[7] and therefore prediction of the effect of the protein fluctuations on the heme is challenging. In the present paper, experimental spectra of cyt *c* are being compared with computations in order to evaluate the importance of particular contributions at physiologically relevant temperatures. Absorption spectra of cyt *c* were taken as a function of temperature for the protein in water, glycerol/water, or trehalose. Trehalose is widely used in nature as a protector of proteins under dehydrating condition.[17] It has been used to study dynamics of heme proteins[18−20] and its physical characteristics have been examined.[21−23] For a low-temperature-forming glass, glycerol/water mixtures are commonly used.[24] The glasses can be made at different temperatures so that the exterior part of the protein becomes rigid at different temperatures, but then the spectra are compared at one temperature. By this means, broadening due to internal motions can be isolated from those motions that are sensitive to the solvent.

* Author to whom correspondence should be addressed. Phone: 215-898-8783. E-mail: vanderko@mail.med.upenn.edu.

† Equal contributions.

10.1021/jp014208y CCC: $22.00
Published on Web 04/30/2002

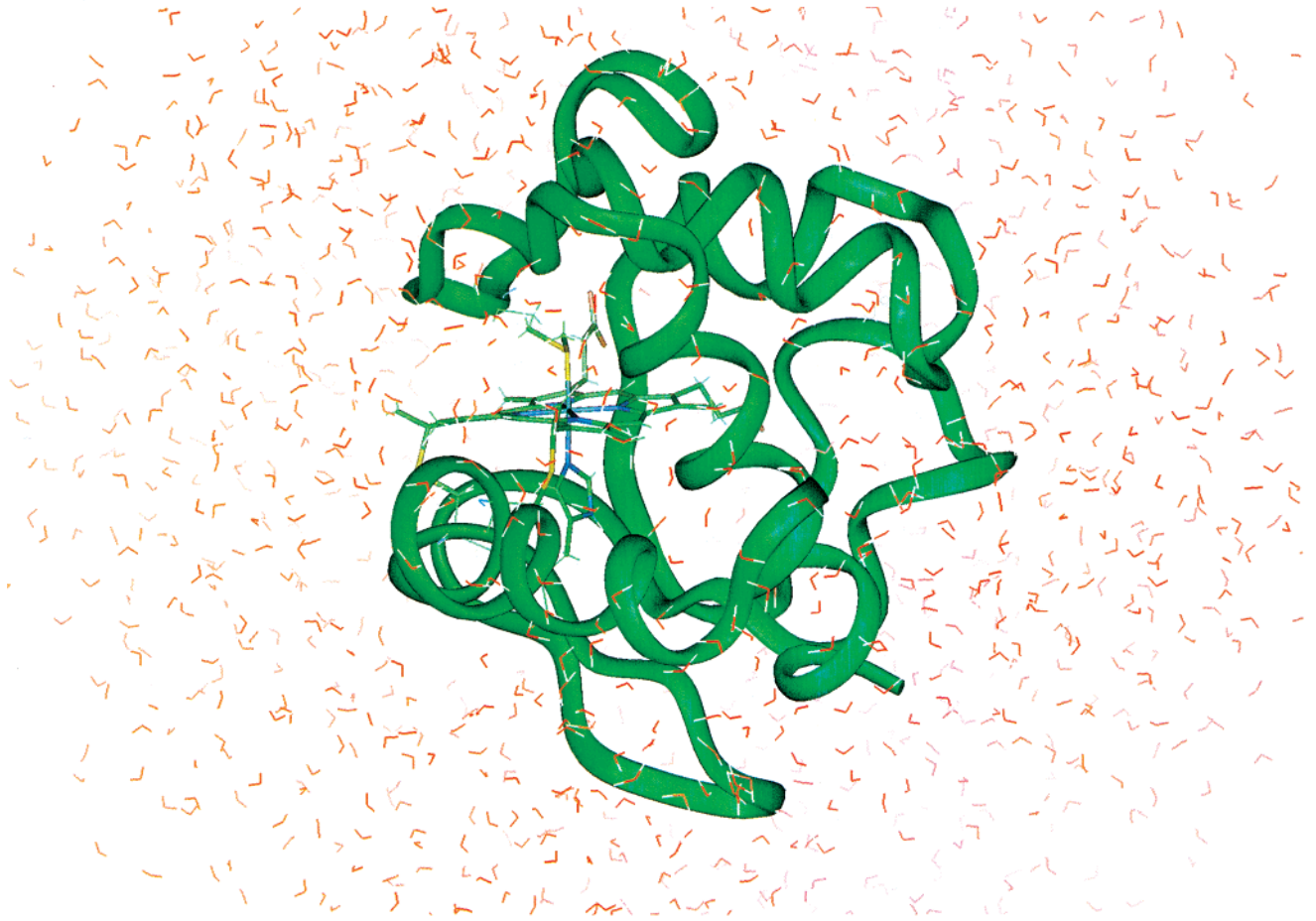

Figure 1. Model system for the MD simulation. The simulation box contains the model cyt *c*, water molecules, and chloride counter-ions. The protein and some of the water molecules are displayed here.

The observed spectral properties are compared with computations of the spectra due to changes in environment produced by protein dynamics. Molecular dynamics (MD) calculations are performed for the sample at a temperature where the spectrum was taken (333 K). Structures obtained from the dynamics simulation are used for analysis by Zindo/S quantum methods. The heme spectra are calculated for the thermally fluctuating sample, and we then compare them with the experimental spectra.

II. Materials and Methods

Experimental Procedures. Horse heart cyt *c* and trehalose were obtained from Sigma Chemical Co (St. Louis MO). Water was deionized and then glass distilled.

Trehalose glass was prepared from supersaturated trehalose solutions as follows. Trehalose (600 mg) was dissolved in 500 mL of distilled water. This solution was heated to ~333 K to ensure complete dissolving of the sugar. Ferrous cyt *c* was added. The solution was placed on a glass slide that was at 333−335 K or at 373 K. The sample was held at the given temperature to allow for evaporation of the water. To prepare the low-temperature glass, the solution was placed on a glass slide at 333 K and allowed to evaporate until the sample was viscous. It was then placed in a 193 K freezer where the water was allowed to sublimate until the sample was dry. All trehalose glass samples were hard to the touch and the samples were brittle. Visual examination under crossed polarizers showed no indication of crystal formation. Some experiments were repeated using 50% trehalose and 50% sucrose. The mixture of sugars prevents crystal formation. The same results were obtained in the pure trehalose and the mixed sugar glasses.

A Hitachi Perkin-Elmer absorption instrument was used to take the visible absorption spectra. IR spectra were obtained with a Bruker IFS 66 Fourier transform IR instrument (Bruker, Brookline MA). A transmission cell holder with a 100 μm spacer and CaF_2 windows was used to hold the sample. The temperature of the sample in both instruments was regulated by a top-loading OmniPlex cryostat (APD Cryogenics, Allentown PA). The spectra were deconvoluted using Peak-Fit (Jandel).

III. Computational Methods

Molecular Dynamics. The starting coordinates of the cyt *c* were from the X-ray structure of Bushnell et al. (1HRC).[25] The force field was described using CHARMM 22[26] (part of CHARMM 27 program suite)[27] for all atom protein parameters. Minor modifications were made to the force field to introduce chemical connectivities that are specific to this protein, viz., the bonds from Cys 14 and Cys 17 to the porphyrin ring and to ensure that Met 80 stays liganded to the central iron. The S−C bond stretching parameters were taken to be 240 kcal/mol with an r_o of 1.816 Å. The S−Fe bond stretch was taken to be 250 kcal/mol with r_o equal to 2.32 Å. The simulation box was cubic with sides of 56 Å and contained a total of 5116 explicit water molecules modeled by TIP3 parameters.[28] The protein charge was balanced by six randomly placed Cl anions that ensured the charge neutrality of the simulation box. The protein molecule and some of its surrounding water molecules are shown in Figure 1.

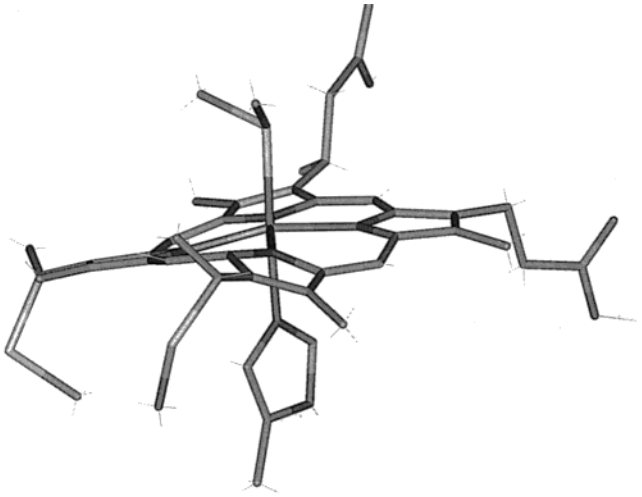

Figure 2. Model cluster (Fe-porphyrin) used in the quantum mechanics simulation. The atoms used in the Zindo calculation are displayed. They consist of the heme, $S-(CH_3)_2$ for Met 80, $Im(CH_3)$ for His 18. Met 80 and His 18 are liganded to the central iron. Also included are two $(S-CH_3)_2$ for Cys 14 and Cys 17, which are bound to the periphery of the heme and anchor it to the rest of the protein. Propionate groups A and B, as defined in the PDB file, are indicated. The coordinates of these atoms are taken from the crystal structure or from the MD simulation, except for the methyl groups which cap the broken covalent bonds to the protein and H atoms used to cap the acidic propionyl oxygen. These groups and the H were built and had their coordinates refined with CHARMM.

The simulation software for MD was CHARMM 27. It uses periodic boundary conditions and the leapfrog Verlet integration scheme and the Berendsen constant temperature algorithm with a coupling constant of 5 ps. All chemical bonds were subjected to holonomic constraints by using the SHAKE algorithm. A time-step of 1 fs was used due to high temperature (333 K) being simulated. The long-range interactions were calculated with a cutoff of 13 Å and incorporating the classical force shift algorithm.

The equilibration included an initial minimization by 50 steps of the steepest descent procedure followed by dynamics while keeping the protein fixed. The whole system was then allowed to move and was gradually heated to 333 K. The velocities of the atoms were then reassigned from a canonical Maxwell distribution at intervals of 10 ps so that the total heating and equilibration procedures were done over a 200 ps simulation time. Structures were taken at every picosecond for 300 ps after the equilibration period for further analysis.

Quantum Mechanics. The cluster of atoms ($FeN_6S_3C_{42}O_4H_{48}$) used in the quantum calculation is shown in Figure 2. It is hereafter referred to as "Fe-porphyrin" and it consists of the heme, $S-(CH_3)_2$ for Met 80, $Im(CH_3)$ for His 18, and $(S-CH_3)_2$ for each Cys 14 and 17. Met 80 and His 18 are referred to as the ligands since these are coordinated to the Fe. The heme plane was oriented in the *xy* plane and the Fe−S Met80 bond aligned along the *z*-axis. A total of 300 different conformations of the cluster were extracted from the dynamics calculations. These structures were used for the quantum chemical calculations utilizing the INDO/s semiempirical method developed and parametrized for spectroscopy in the ZINDO program as implemented in the Cerius 2 software package (Molecular Simulations, Inc., Sherrills Ford, NC). Singles configuration interaction (SCI) was used in conjunction with the INDO/s method to calculate optical spectra.

To evaluate the effect of the charges in the surrounding protein atoms on the optical spectra we built a second set of systems consisting of Fe-porphyrin described above and partial charges placed at the positions of the remaining atoms in the protein. This system is hereafter referred to as "Fe-porphyrin-Q". The partial charges of 1647 atoms of the protein were taken from the CHARMM force field and are the same as used in the MD simulation. The electrostatic field generated by the protein is incorporated into the quantum mechanical calculation of the spectra.[6] This is an advance over using just formal charges, or formal charges plus partial charges from the amide groups.

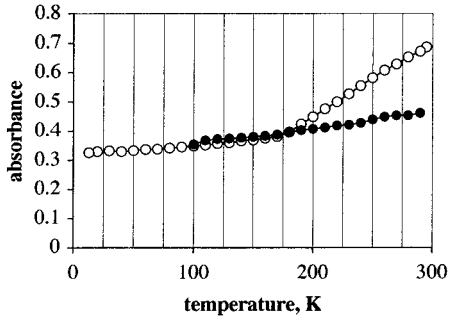

Figure 3. OH-stretch region of the solvent as a function of temperature. Absorbance at 3500 cm^{-1} for glycerol/water (60/40 w/w) shown with open circles. Closed circles shows the absorbance at 3400 cm^{-1} for trehalose glass.

The results can, in principle, be improved with an increase in the numbers of atoms used in the quantum calculations. There has been a progression in the literature in the sophistication of the calculation, starting from considering only planar porphine, then including ligands and side chains.[29,30] We now include the propionic acids and the S from the covalently bond Cys. In our procedure we make no assumptions about the symmetry of the heme, because the quantum mechanical INDO calculation takes into account all distortions from square-planar symmetry. Further advance would be to include more atoms, or indeed all atoms of the protein, in the computational cluster,[31] but since many dynamical structures are considered, this approach is presently computationally intractable.

IV. Results

Characterization of the Solvents and the Protein/Solvent Interactions. IR spectroscopy was used to get information on the nature of the solvent, and the interaction of the solvent with the protein.

The IR spectrum of the trehalose glass was measured, and the peak at 2945 cm^{-1}, which represents the C−H stretch of trehalose, was used to determine the amount of trehalose present. The HOH bending mode at 1642 cm^{-1}, which shifted to 1670 cm^{-1} in the glass, was used to estimate the water content. About 1.8 to 2.2 molecules of water/molecule of trehalose was found. This is close to the value found by Librizzi et al. using other IR bands.[32]

The OH stretch band of water and aqueous alcohols represents a strongly absorbing group. This band shifts to lower frequency and increases in intensity as temperature decreases.[33] By recording the absorbance at one frequency of this band, changes in the glass as a function of temperature can be monitored. Changes in the OH stretch extinction of trehalose and glycerol/water are shown in Figure 3. The OH stretch absorption allows us to identify the glass transition at 180 K for the glycerol/water solvent. In contrast, the trehalose OH band remains relatively temperature independent over the range, showing the constancy of the glass structure.

The IR spectra of Fe(II) cyt *c* in trehalose is seen in Figure 4A. The peak at 1620 cm^{-1} represents the amide I band, and

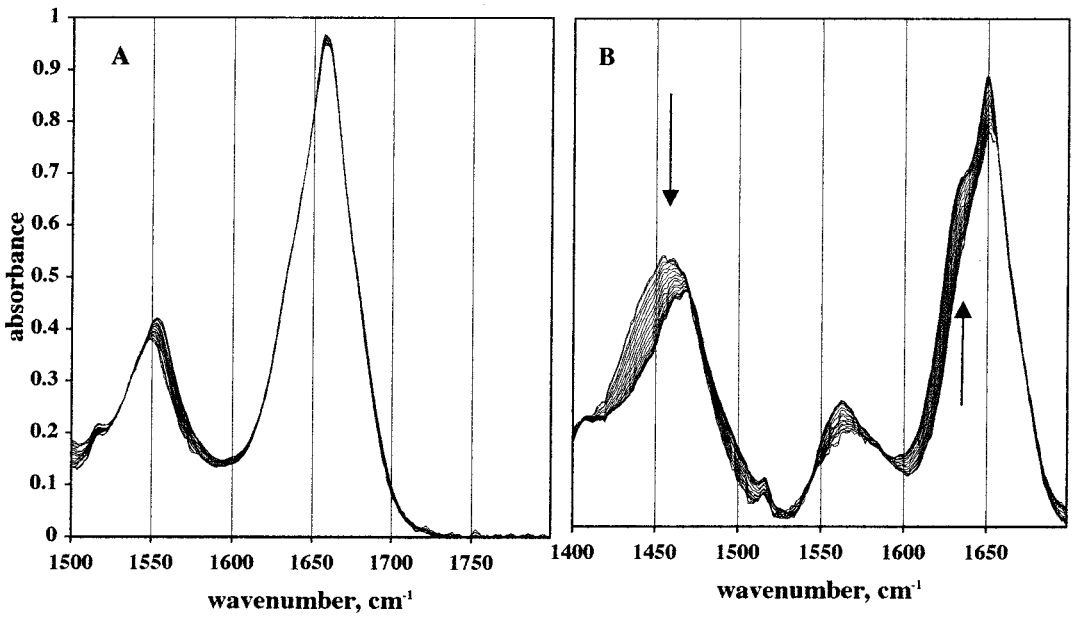

Figure 4. Infrared spectra of the amide region of cyt *c*. (A) cyt *c* in trehalose. (B) cyt *c* in deuterated glycerol/D_2O (60/40 w/w). Arrows indicate the amide I′ and I″ region. Temperature range: 100 to 300 K.

this band is characteristic of hydrated amide groups, as reported previously for dried protein in trehalose.[34] The amide I peak is constant with temperature change whereas the amide II band at 1550 cm^{-1} shifts slightly to higher frequency from room temperature to low temperature. The IR spectra of Fe(II) cyt *c* in D_2O/glycerol is given in Figure 4B. We have previously noted that the amide I′ prime band shows additional absorbance at lower frequency as the temperature decreases. This was attributed to a strengthening of the H-bond between water and solvent-exposed helical regions.[35] The changes in the spectra then are taken to indicate water/protein interactions. Over this same range the amide II′ band at 1450 cm^{-1} also shifts in the same direction for cyt *c* in D_2O/glycerol.

Absorption of Fe(II) cyt *c*. Absorption spectra of Fe(II) cyt *c* in glycerol/water at temperatures from 333 to 10 K are shown in Figure 5. In Figure 6 spectra for the protein in trehalose glass prepared at 333 K are shown in the same range. In both cases there is a shift to higher frequency and an increase in absorbance in the Q(0,0) region as the temperature decreases. As the temperature is lowered, the spectral bands become narrower, and at the lowest temperature, the Q(0,0) region splits into two bands (apparent as a shoulder in Figure 6).

The spectral widths of the $Q(0,0)_x$ band were analyzed over the entire temperature range. The results are summarized in Figure 7 for three trehalose glass conditions (formed at 373, 333, and 193 K), for water (data only for 293 to 333 K) and for glycerol/water. (Similar width changes were seen in the $Q(0,0)_y$ band). Looking first at 293 to 333 K, it can be seen that the widths of the bands are nearly the same for water (solid squares), for glycerol/water (open circles), or for the protein in the trehalose glass formed at 193 K (open squares). This indicates that glycerol/water in the liquid state or trehalose in the solid state has only a small direct effect on the heme, which is located in the interior of the heme. Now focusing on the width for the protein in glycerol/water and for the protein formed in trehalose glass formed at 193 K, it can be seen that the temperature profiles over the range of 10 to 373 K are remarkably the same. This is an interesting comparison, because, as shown above, the glycerol/water mixture forms a glass close to the temperature used for forming this trehalose glass. The sample for glycerol/water is liquid above 200 K, whereas the sample in the 193 K trehalose glass is solid (see Figure 3), yet the $Q(0,0)_x$ bands show almost the same widths at high temperature. This is consistent with the view that at high temperature, the internal dynamics are the main source of inhomogeneity. Finally, the widths of the absorption narrow as the temperature decreases even for the glass formed at 333 and 393 K, but at all temperatures the bands are narrower for the protein which was incorporated into a matrix with a lower temperature glass

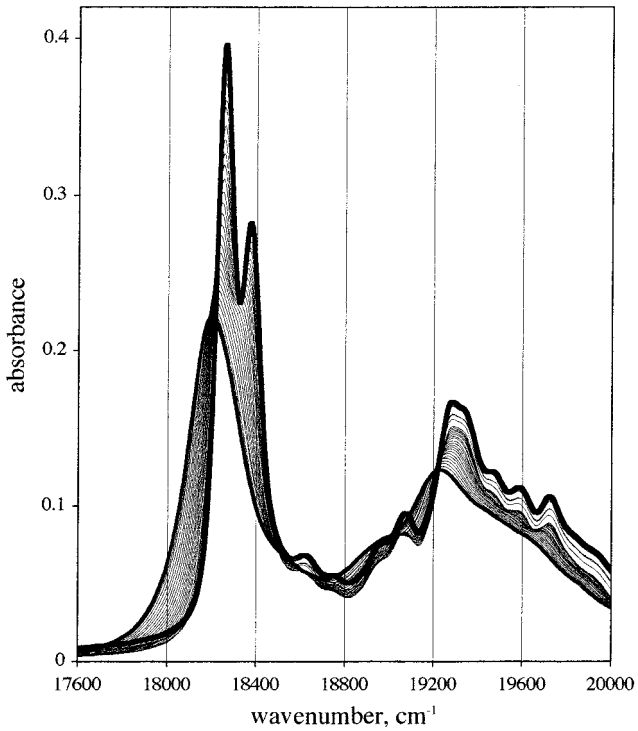

Figure 5. Absorption of Fe(II) cyt *c* in glycerol/water from 330 (dark broad spectrum) to 10 K (dark narrow spectrum). All spectra were taken at 10 degree intervals. The band at 18200 cm^{-1} at room temperature represents the Q(0,0) band; the split at low temperature is evident in the band between 18100 and 18400 cm^{-1}. The lower frequency is defined as the $Q(0,0)_x$.

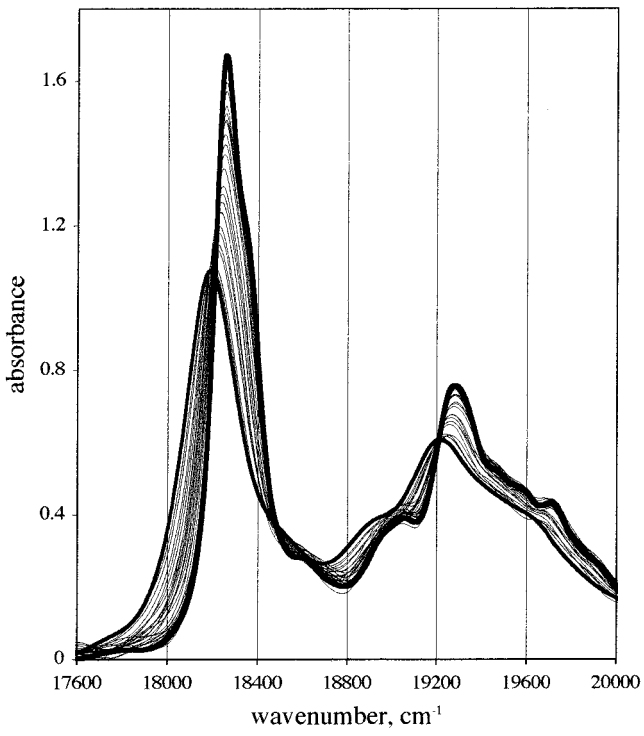

Figure 6. Absorption of Fe(II) cyt *c* in trehalose glass at temperatures from 330 (dark broad spectrum) to 10 K (dark narrow spectrum). All spectra were taken at 10 degree intervals. Trehalose glass was prepared at 333 K.

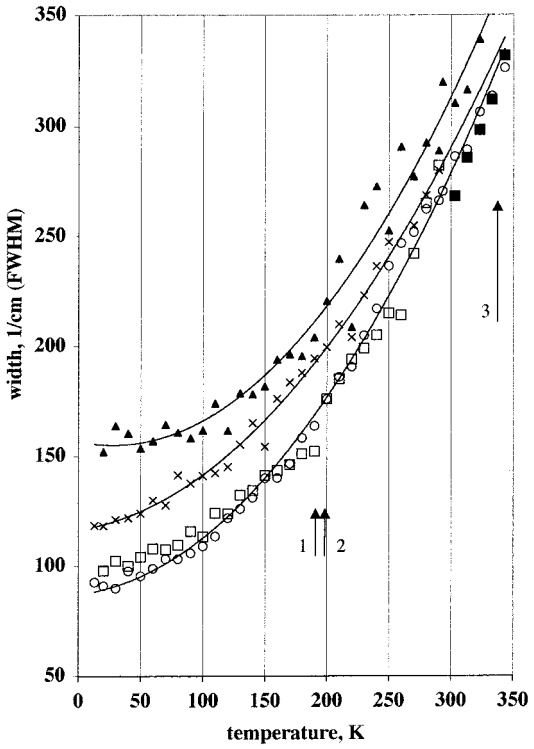

Figure 7. Absorption widths of the $Q(0,0)_x$ band of Fe(II) cyt *c*. The protein was in the following matrix: closed squares: water; open circles: 60% glycerol/water (glass transition indicated by arrow 1); open squares: trehalose formed at 193 K (glass formation temperature indicated by arrow 2). x: trehalose formed at 333 K (glass formation temperature indicated by arrow 3); closed triangles: trehalose formed at 373 K. Lines are polynomial fits and serve only as a visual aid.

transition. Comparing the spectra taken at the lowest temperature shows this. At 10 K, the width of the $Q(0,0)_x$ band is ~150 cm^{-1} for the sample which was entrapped in glass formed at 373 K. The width is ~80 cm^{-1} for the protein in glass formed at low temperature.

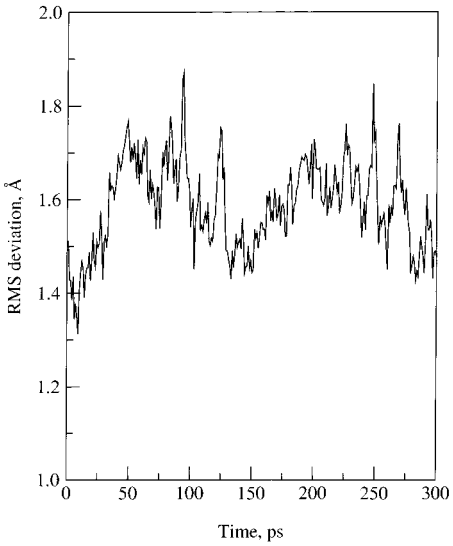

Figure 8. Fluctuations of the protein atoms in the MD simulation. The RMS deviation of structures at every picosecond are calculated as a function of time after orienting the molecule with respect to the X-ray structure.

Molecular Dynamics of cyt *c*. Using molecular dynamics simulation we approach the question of what in the protein causes the thermal broadening of the spectra.

As indicated in the Computational Methods section, structures at every picosecond for 300 ps after the equilibration period were used for the analysis. As seen in Figure 8 the root-mean-square (RMS) deviation of the protein as measured with respect to the X-ray structure oscillates around an average value of around 1.6 Å, indicating that the model protein is not denaturing. The high value of the average RMS deviation may be due to differences in the protein's structure in the crystal and solution environments.[36,37] The large oscillations are in part due to high-temperature being used. They vary between values of 1.3 and 1.9 Å, implying that the model protein rapidly interchanges between various conformational substates, thus justifying the use of the high temperature in this simulation.[37] The average value of RMS deviation for only the backbone atoms of the protein is 1.25 Å/atom, which is also the value at the end of the equilibration.

The distribution of the RMS deviation of particular parts of the protein is examined in Figure 9. Considering only the porphyrin ring portion of the heme, the distribution is narrower (Figure 9A solid line) than for the entire heme including side groups and propionic acids (Figure 9A, dotted line). A large contribution to the RMS is due to the movement of the propionic groups. In Figure 9B the distribution in the RMS deviation for the propionic acid groups is seen to range between values of 0.25 Å and 1.25 Å from the X-ray structure. The RMS deviation is larger for carboxylate A than for B. Carboxylate A is more associated with water, as seen from its association with water over the entire trajectory time (Figure 9 B, inset).

Spectral Features Determined by Quantum Mechanics. The molecular dynamics show that both the heme cluster and the surrounding polypeptide chain undergo fluctuations. The 300 structures from the 300 ps dynamical simulation shown in Figure 8 were used to calculate the spectral transitions and splitting of the Q(0,0) band using the ZINDO software. The computer programs allow us to examine what causes the large spread in

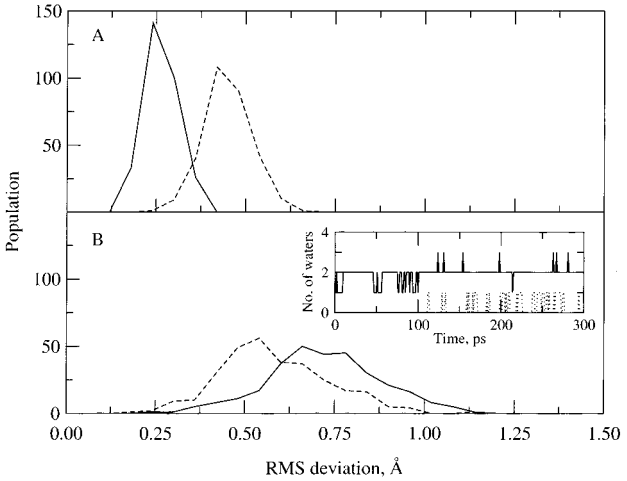

Figure 9. Fluctuations in the coordinates of moieties in the MD simulation. The populations of RMS deviation calculated from the MD simulation are shown. The populations were calculated for intervals of 0.6 Å. The RMS deviations were calculated after orienting the heme coordinates of the MD simulation structure with respect to the heme coordinates from the crystal structure.[25] (A) Populations of the RMS deviations for only the heme ring structure (solid line) and for the heme structure with the peripheral groups including the propionic acids. (B) Populations of RMS deviations for propionic group A (solid) and propionic group B (dashed). Inset: The number of waters in proximity to the propionic groups. The time course shows the number of water oxygen atoms within 3.3 Å of either of the acidic oxygen atoms of propionic group A (solid line) and propionic group B (dashed line) are displayed.

the calculated transition energies. The time sequences of the calculated splittings are shown in Figure 10. In Figure 10A, the calculated splitting due to the dynamics of Fe-porphyrin is shown. In Figure 10B the difference in the calculated splitting between the Fe-porphyrin-Q and Fe-porphyrin is plotted for each structure. The influence of the matrix is seen to increase the splitting in some cases by values of more than 300 cm^{-1}, and spikes even larger than that. At the same time there is a decrease of more than 300 cm^{-1} in others. It is also observed that these values fluctuate in such a way that, on average, there is a cancellation in the large positive and negative influences on the splitting.

The influence of the changes in the electric fields generated by the protein matrix was examined further. To do this, the coordinates for the heme cluster was held fixed, but the positions of the protein charges were obtained from the molecular dynamics trajectory (Figure 10C). Using the heme coordinates from the crystal structure, the dynamics of the polypeptide chain is predicted to cause spectral broadening, since there are fluctuations of the calculated splitting, but the magnitude is smaller than if compared with the splitting obtained due to the dynamics of Fe-porphyrin (Figure 10A). It can be seen that the protein fluctuations also influence the splitting (Figure 10B), but that the effect is not as large as when the dynamics of the cluster is considered (Figure 10A).

The calculated values of the two spectral transitions, $Q(0,0)_x$ and $Q(0,0)_y$, for Fe-porphyrin show a significant spread when its dynamics is considered (Figure 11). Both distributions have Gaussian-like bell shapes. The lower energy transition is centered at 15826 cm^{-1} and ranges between values of around 14900 and 16600 cm^{-1}. The higher energy transition is centered at 16207 cm^{-1} and ranges between 15400 and 17500 cm^{-1}. The average value of the spectral splitting for these structures was 380 cm^{-1} which is well above that calculated for the splitting of the X-ray structure (~27 cm^{-1}) from the current set of

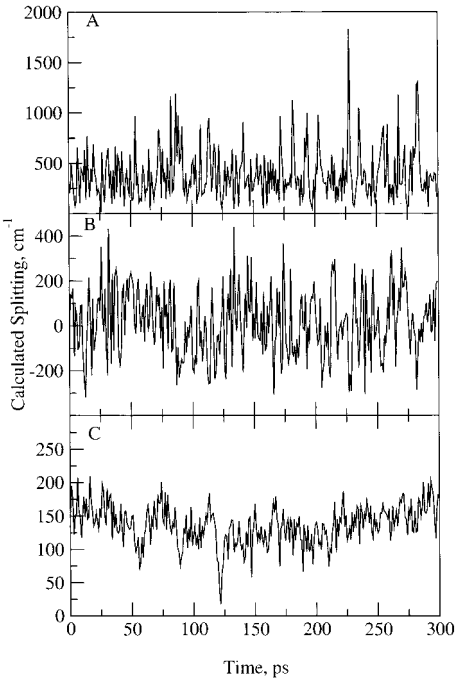

Figure 10. Time sequence of the calculated splittings. The splittings are calculated as described in the Text. (A) The calculated splittings due to the dynamics of Fe-porphyrin. The coordinates for the cluster are built from the time frames from the MD simulation. (B) The difference between the calculated splitting for Fe-porphyrin-Q and Fe-porphyrin. The coordinates for the cluster and the protein charges are obtained from the MD simulation. (C) The splitting energy is calculated for the cluster having coordinates of the crystal structure but with the protein charges having coordinates taken from the time frames of the MD simulation.

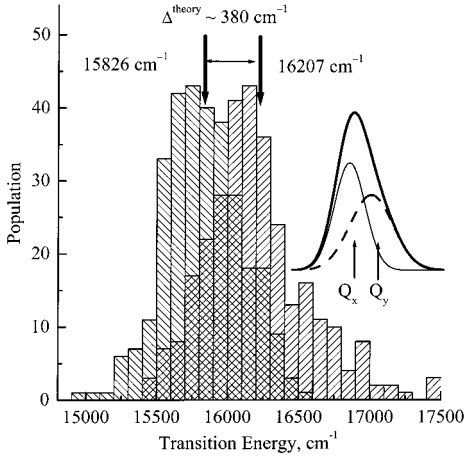

Figure 11. Effect on the optical transition from the distortions of the atoms in the cluster, Fe-porphyrin. Populations of calculated transition energies were calculated for the structures from the dynamics simulation. The populations of the two calculated transition energies for the MD generated structures are displayed. The two splitting energies for the Q(0,0) band were calculated using ZINDO and the populations of each transition were determined for the intervals of 50 cm^{-1} and the two resultant histograms are shown. Inset: The calculated spectrum of cyt *c* at 333 K. Gaussian functions were calculated using the height and width of each of the two population distributions described in the figure and in the text. The ratios of intensities between $Q(0,0)_x$ (solid line) and $Q(0,0)_y$ (dotted line) is 0.7 and is the mean value over the 300 calculations. The bold-solid line is obtained by adding the spectra for $Q(0,0)_x$ and $Q(0,0)_y$ transitions.

approximations and computational parameters. The Gaussian functions, shown in Figure 11 inset, were drawn using the

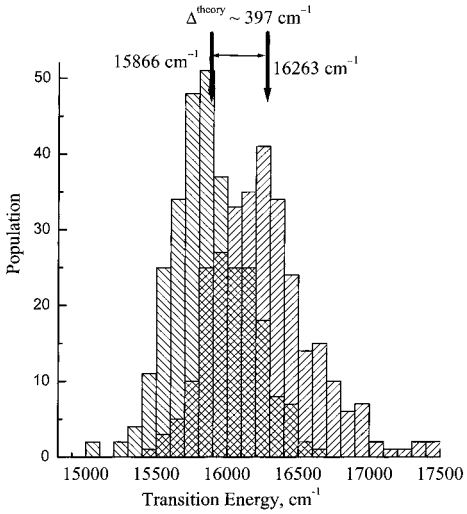

Figure 12. Effect on the optical transition including distortions of the heme and the fluctuation electric field due to charges of the protein, Fe-porphyrin-Q. Populations of calculated transition energies were calculated for the structures from the dynamics simulation. Lower transition and upper transition are distinguished by angle of the shading.

population distribution of molecules and the calculated absorption extinction, and this is what is comparable to the experiment. It can be seen that the extinction coefficient of the low-frequency band is lower than for the high-frequency band. The ratios of intensities between two Gaussians is 0.7, which is the mean of the 300 quantum calculations.

On including the electric potential due to the partial charges on the protein atoms surrounding the heme (i.e., Fe-porphyrin-Q), bell-shaped distributions are once again seen for the transitions (Figure 12). The centers of the distributions for the two transitions are 15866 and 16233 cm^{-1}, which are 40 and 32 cm^{-1} higher in energy than for the uncovered heme cluster. The average value of the spectral splitting is 397 cm^{-1}, which is only about 17 cm^{-1} higher in energy than for Fe-porphyrin. The overall distributions for both transitions are fairly similar for Fe-porphyrin and Fe-porphyrin-Q, though a proportionally larger number of transitions in the high energy regions near 17500 cm^{-1} are observed in Fe-porphyrin-Q.

Lack of Correlation in the Frequencies of the Q(0,0)$_x$ and Q(0,0)$_y$. Overall, it is observed that the transition energies and the splitting are very sensitive to changes in the structure of Fe-porphyrin. The sensitivity to changes of the electrostatic potential due to the dynamical motions of the protein, though not as pronounced, is also definitely significant. If there would be a simple factor causing the splitting then one might expect that molecules that would show deviation from the unsplit form in the Q(0,0)$_x$ would show the same deviation in the Q(0,0)$_y$. Therefore, one might expect that there would be an inverse correlation between the Q(0,0)$_x$ and Q(0,0)$_y$ frequencies. An experimental means to examine this is with a hole-burning experiment.[38,39] The experiment is described in the inset of Figure 13. If there is a correlation between the two bands, destruction of one sub-population by laser irradiation in the Q(0,0)$_x$ band will produce a hole in the Q(0,0)$_y$ region. If there is no correlation, then there will be a diminution of the entire Q(0,0)$_y$ region. In our simulations, we found that there was no significant correlation. This is demonstrated in Figure 13, where molecules having a Q(0,0)$_x$ frequency between 15800 and 15900 cm^{-1} were removed. There was a decrease in the population of molecules over the entire Q(0,0)$_y$ band.

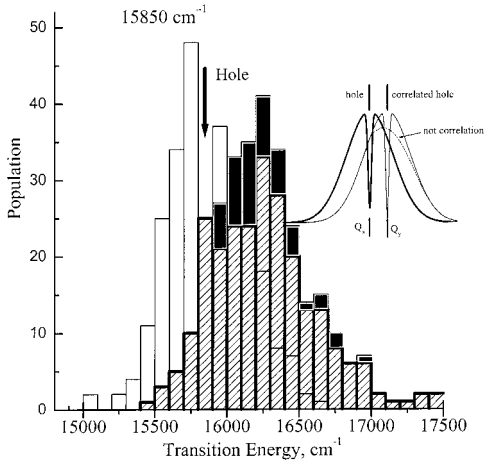

Figure 13. Effect of removal of one population on the observed spectrum. Open bars represent the population of Q(0,*0*)$_x$y and hatched bars the population of Q(0,0)$_y$. Data are the same as presented in Figure 12, but molecules with a Q(0,0)$_x$ transition energy between 15800 and 15900 cm^{-1}, indicated by arrow, were removed. The dark bars in the Q(0,0)$_y$ region represent those molecules that were also removed by formation of the hole in the Q(0,0)$_x$ region. Inset: diagram to explain hole burning. The dark line is the distribution of transitions for the Q(0,0)$_x$ region, with the hole indicated. For perfect correlation, a hole will be seen in the Q(0,0)$_y$ region (indicated by narrow line). For no correlation, the Q(0,0)$_y$ band will decrease, indicated by the dotted line.

V. Discussion and Conclusions

Protein Interaction with the External Matrix. An enduring question is the relationship of protein internal motion to the solvent viscosity. In our experiment we used trehalose to form glasses at various temperatures. Trehalose has a known protecting effect on proteins[17,40] and it is used in nature by lower organisms for protection against anhydrobiosis.[41] As a structure breaker of the H-bonded network of water, it acts to prevent crystallization.[23,42] Therefore, in addition to providing a solid matrix for the protein, the trehalose/protein glass system has biological relevance.

The IR spectra shown here (Figure 4A) represent some of the most compelling evidence to account for protein protection by trehalose and the interaction of trehalose with the protein. The figure shows that the protein amide I group remains constant over a temperature range of almost 200 degrees. In contrast, the amide peak of the protein in glycerol/water shows increased absorbance at the lower frequency region of the amide I′ band (around 1630 cm^{-1} in Figure 7B) with lowered temperature. H-bonding of the mobile water molecules strengthens as temperature decreases,[33] and it was suggested that the shift in the spectrum reflects an increase in the H-bonding strength between solvent and the carbonyl of the amide group as temperature decreases.[43] This idea was substantiated by isotope labeling of exposed and buried amide groups.[35]

Following this reasoning, the constancy of the amide I′ band with temperature for the protein in trehalose shows that the H-bonding of the protein to trehalose (and residual water) does not change with temperature. The trehalose may be H-bonded to the amide links, but the rigid matrix does not move with temperature. The rigidity of the matrix is indicated by the constancy of the OH stretch (Figure 3). The protein is therefore unable to undergo large-scale fluctuations, and it is protected against denaturation.

Spectral Changes of the Q(0,0) Band as a Function of Glass Transition. Figure 7 shows three interesting characteristics of temperature/solvent effects: (i) at the higher temper-

atures the spectral widths are independent of the solvent and show the same temperature dependence; (ii) there is no sharp discontinuity at either the glycerol/water or trehalose glass transitions; (iii) at the lowest temperatures, where all the solvents are glassy, the width is constant and reflects the temperature at which the glass was formed, i.e., greater width seen in the samples formed at higher glass temperature.

We can interpret these features in terms of contributions to the spectral width from two types of protein fluctuations: a contribution from solvent-coupled motions, and a contribution from motions uncoupled from solvent motions. The contributions from the coupled motions will be frozen in at the temperature at which the solvent forms a glass, will have little temperature dependence below this temperature, and their contribution to spectral broadening will reflect the magnitude of these fluctuations at the solvent glass temperature. The uncoupled fluctuations are independent of solvent type, and so at a given temperature give a similar contribution to broadening irrespective of solvent composition, and similar temperature dependence. Moreover, since they are uncoupled to the solvent, their contribution to spectral broadening continues to decrease as the temperature is lowered, even if the solvent is a glass.

In this model at higher temperatures uncoupled motions provide the largest contribution to broadening, explaining the independence from solvent type at high temperature. As the temperature is lowered, the contribution from uncoupled motions continually grows smaller. The contribution from the coupled motions will also decrease with temperature until the solvent glass transition, at which point it has little temperature dependence. However, the sharp transition in temperature dependence from solvent-coupled contributions is masked by the smoothly decreasing contribution from the uncoupled term. This explains the absence of a sharp discontinuity. Finally, as the temperature is lowered further, the uncoupled contribution continually decreases, and the spectral width is increasingly dominated by the frozen-in contribution from solvent-coupled motions. This accounts for the divergence of the curves in Figure 7 at low temperature, and their "bottoming" out at a value dependent on the solvent glass transition temperature.

In this model it is necessary to explain how there can be motions that are uncoupled to the solvent, which can provide a significant contribution to spectral broadening, and which show a temperature dependence down to low temperatures, even when the solvent is frozen. Analysis of the contributions to the potential at the heme from different parts of the protein (Figure 14) provides a clue. Analyzing the MD simulations at 333 K, the mean contribution to the potential at the heme from each protein atom, its RMS fluctuation, and the average solvent exposed area for each atom is plotted against the distance of that atom from the heme group. The bars show that atoms farther from the heme undergo a larger fluctuation, have a higher accessibility to solvent, and are presumably increasingly coupled to the solvent. These motions would be sensitive to the solvent viscosity. However, their contribution to the potential at the heme, indicated by the dark bar, and thus their contribution to spectral broadening is smaller at large distances at 333 K. Conversely, atoms close to the heme undergo a smaller fluctuation, yet because of their closeness, make a larger contribution to the potential (and its fluctuation) at the heme. It is these smaller motions in atoms close to the heme that would provide the solvent-independent contribution: Since they involve relative small motions in buried atoms they would show a significant temperature dependence even down to low temperatures and would not be "frozen-in" when the solvent formed a glass.

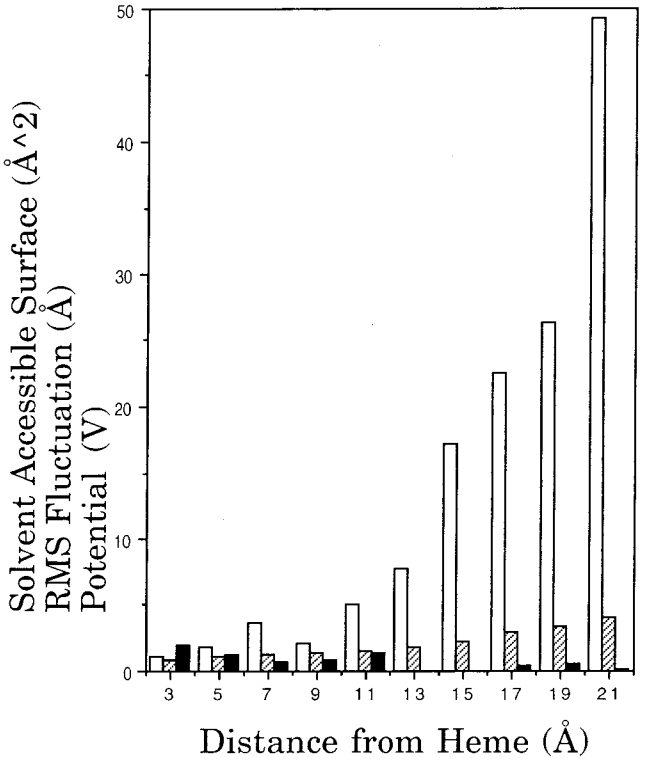

Figure 14. Plot of mean solvent accessible area of atoms (unshaded bar), root mean square fluctuation (hatched bar), and mean contribution to electrostatic potential at the heme (solid bar), as a function of their distance from the heme cofactor.

The above interpretation of the results is consistent with results for the kinetics of CO binding to myoglobin. In this case, the escape of CO from the heme pocket is prevented at room temperature.[20,44,45] At the same time, the width of the Soret band narrows at low temperature[19] and the distribution of tryptophan lifetimes indicates that large-scale protein fluctuations decrease.[44] These results point to retention of the dynamics of the protein, which has been suggested to be possibly due to retention of internal waters in the trehalose glass.[46] The optical bandwidth of carbonmonoxy-horseradish peroxidase is likewise little affected by the presence of trehalose, and reflects the internal dynamics and low-lying states of the protein.[47]

Correlation of Spectra with Dynamics and Quantum Computation. To interpret the spectral results we use a combination of molecular dynamics and quantum calculations. The relationship between dynamics of cyt *c*, electron transfer reactions, and the incorporation of the average electrostatic properties due to conformational changes have previously been studied by Warshel and co-workers.[48,49] In a later study more closely related to the work described here, they considered the contribution of protein-induced electric potential fluctuations to the electron-transfer reorganization energy.[50] Recently, Sharp[51] obtained very similar reorganization energies using the finite difference Poisson−Boltzmann method, demonstrating the utility of both approaches in studying the effect of protein fields on the heme properties. In this work, we have extended the approach to study the protein's effect on heme absorption spectra.

Assuming the Franck−Condon approximation, in an absorption spectroscopy experiment the spectrum represents the static distribution of the molecules. The observed spectrum is a function of the distribution of the transition energies of the

hemes at the given temperature. Therefore, from the molecular dynamics simulation and quantum mechanical calculation, we now turn to the predicted distribution of energies and the splitting of the Q(0,0) band.

The heme of cyt *c* is distorted from planarity in a manner conserved for all cytochrome *c* types.[52,53] The distortion is seen in Figure 2. Consistent with the rigidness of the planar group and its burial within the protein (Figure 1) the RMS deviation for the heme group is small (Figure 9A). When the heme peripheral groups including the propionic acids are included, the RMS deviation is larger. Since the propionic acids are one contact of the heme with the solvent, this effect was examined in more detail. In Figure 9B, the RMS deviation for the two propionate groups is seen. The two propionic acid groups interact with water differently, see Figure 9B inset, with the interaction of the propionic acid group A being stronger. Water molecules were observed in recent MD simulations to exchange from the aqueous bulk to the interior of the protein in time-scales varying from a few picoseconds to nanoseconds and also to show diffusion within the protein interior.[54] Although the RMS deviations of the heme are small (Figure 9A), changes in the chromophore itself have a large effect on the optical properties (Figure 10A). In Figure 10B, the splittings due just to the protein electric field effects are presented. Because the fluctuations in the cluster itself cause such a large effect, it is not apparent that the fluctuations of the atoms of the polypeptide chain, which produces a change in the electric field at the heme, affects the spectrum. However, when one structure is taken, as in Figure 10C, the polypeptide chain is shown to have a positive effect on the splitting. We note that our calculations can in principle be improved by replacing the CHARMM classical potential energy surface of the heme with a better one: ideally, a full quantum dynamical treatment of the entire protein/heme. This is currently computationally prohibitive for a system of this size. Hybrid methods combining quantum mechanics and molecular mechanics are available for the study of proteins.[55−57] These QM/MM methods provide a better description of the heme energy surface than the empirical force field we have used to obtain our dynamics trajectory, and they may be the methods of choice when it becomes computationally tractable to calculate dynamics trajectories as long as those in this study.

To compare the computations with spectral measurements, the computations are consistent with the inhomogeneous broadening and closely lying energetic states indicated by hole burning in cyt *c* derivatives.[58,59] The Q(0,0) bands are correctly predicted to show inhomogeneous broadening that at high temperature obscures the splitting. Experimentally, the splitting can be seen directly in the spectra when the temperature is reduced (Figures 3 and 4), as a consequence of the reduced fluctuations. However, the splitting arising from the asymmetry of the heme is also seen at room temperature for ferrous cyt *c* using magnetic circular dichroism[60] or Raman polarization[61] and therefore the apparent single band at room temperature is really composed of two bands, as foreseen by the simulations. The simulations predict a correct order of magnitude for the inhomogeneous distribution. The experimental value is around 300 cm^{-1} (Figure 5), close to the calculated value (Figure 11). The calculations also indicate that there will be little correlation between the $Q(0,0)_x$ and $Q(0,0)_y$ frequencies (Figure 13). This was experimentally surmised from hole-burning experiments for another porphyrin−protein system.[62]

We have concluded that spectral broadening in cyt *c* reflects mostly the distortions of the heme produced by thermal activity, but it is possible that this will not be a general feature for all heme proteins. The polypeptide chain of cyt *c* has a fundamental function to stabilize the reduced form, in which the Fe-heme has no net charge. By stabilizing the uncharged form, the protein acts to raise the redox potential of the iron, so that the protein can properly function as a redox carrier between cytochrome oxidase and cytochrome *c* reductase. To do this, cyt *c* needs a relatively hydrophobic heme pocket. Since the electric field falls off rapidly with distance, charged groups farther away have relatively little effect on the spectral features. Surface charges, for instance, were found to have little influence on the redox potentials of Fe−S as compared to charges in the interior nearer the redox center.[63] The arrangement of the heme pocket is not the same for other heme proteins. In both horseradish peroxidase and myoglobin, a small extrinsic ligand molecule must reversibly bind to the iron. The ligand−Fe bond needs to be stabilized by the protein, and charged and H-bonding groups provide the stabilization. For horseradish peroxidase a hydrogen-atom donor must additionally be accommodated near the heme. Work with this peroxidase shows that the electric field produced by amino acids or substrates near the heme has a large effect on the optical spectra[64] and molecular dynamics and electrostatic calculations suggest an effect of the protein electric field on the heme.[65] Finally, we point out that while the procedures used here give insight into the origin of the inhomogeneous broadening, they are not presently adequate to predict the entire spectra. Other analysis procedures are being used to predict vibrational and vibronic spectra.[66−70]

In Conclusion. By examining protein samples that were prepared in glasses formed at different temperatures we can see that the inhomogeneous line widths depend on the temperature at which the glass was formed. The very similar temperature profile for the protein in various glasses suggest that the optical spectral widths of the $Q(0,0)_x$ band of ferrous cyt *c* are largely due to internal motions of the heme group. This is substantiated by MD and quantum calculations of the spectra. The quantum calculations predict that the sample is inhomogeneously broadened and that the Q(0,0) transition is split.

Acknowledgment. The National Institute of Health grants PO1 GM48310 and RO1 55004 supported this work. We thank G. Guffanti for help with some experiments and Drs. P. Angiolillo, A. Kaposi, and S. Stavrov for helpful discussions. The Appendix was prepared by N.V.P., S.D.D., K.S., and J.M V.

Appendix

Effect of Dielectric Constant on Calculated Heme Optical Splitting. The choice of the models for the charges on the protein matrix and an appropriate effective dielectric constant for the protein environment needed to be ascertained.

Two models for charges were tested. In one model, formal charges were assigned to the charged residues as in earlier work from these laboratories. In another model partial charges were assigned to all the atoms of the protein matrix which were taken from the CHARMM parameters. The effect is shown for dielectric 1 to 80, although the value of the dielectric constant for the protein matrix is usually expected to be between 2 and 15. In the absence of accurate data for cyt *c*, a range of dielectric values was tested along with the two models for the charges. The coordinates of the crystal structure were used for the calculation.

In Figure A1, the value of the splitting is around 160 cm^{-1} when the CHARMM partial charges are used and drops exponentially to around 50 cm^{-1} where the dielectric constant

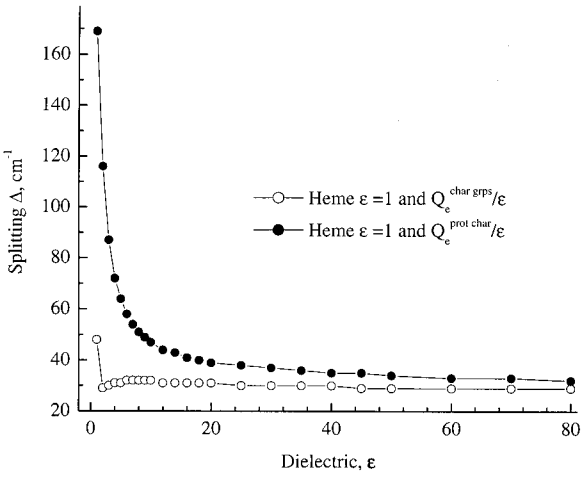

Figure A1 . Dielectric effect. Splitting of the X-ray structure predicted as a function of the medium dielectric. Open circles: The protein environment is modeled with partial charges corresponding to the CHARMM parameter set. Closed circles: The protein environment is modeled with formal charges corresponding to the CHARMM parameter set.

is 15. The value at $\epsilon = 2$ is 116 cm^{-1}, which is very close to the experimental value.

The value of the splitting when the formal charges model is used is 50 cm^{-1} with $\epsilon = 1$ and this drops as the dielectric constant is increased. As expected, as e increases, the influence of the charged groups on the splitting becomes less important.

The models with partial charges from the CHARMM parameter set and a constant dielectric of 2 is used in this work to incorporate the effect of Coulombic energy due to the charges on the protein matrix.

References and Notes

(1) Keilin, D.; Hartree, E. F. *Nature* **1949**, *164*, 254−259.
(2) Wagner, G. C.; Kassner, R. J. *Biochem. Biophys. Res. Commun.* **1975**, *63*, 385−391.
(3) Reddy, K. S.; Angiolillo, P. J.; Wright, W. W.; Laberge, M.; Vanderkooi, J. M. *Biochemistry* **1996**, *35*, 12820−12830.
(4) Hagihara, B.; Oshino, R.; Iizuka, T. *J. Biochem.* **1974**, *75*, 45−51.
(5) Manas, E.; Vanderkooi, J. M.; Sharp, K. *J. Phys. Chem. B* **1999**, *103*, 6334−6348.
(6) Manas, E. S.; Wright, W. W.; Sharp, K. A.; Friedrich, J.; Vanderkooi, J. M. *J. Phys. Chem. B* **2000**, *104*, 6932−6941.
(7) Rasnik, I.; Sharp, K.; Fee, J. A.; Vanderkooi, J. M. *J. Phys. Chem. B* **2001**, *105*, 282−286.
(8) Northrup, S. H.; Pear, M. R.; McCammon, J. A.; Karplus, M. *Nature* **1980**, *286*, 304−305.
(9) Northrup, S. H.; Pear, M. R.; McCammon, J. A.; Karplus, M.; Takano, T. *Nature* **1980**, *287*, 659−660.
(10) Henry, E. R.; Eaton, W. A.; Hochstrasser, R. M. *Proc. Natl. Acad. Sci. U.S.A.* **1986**, *83*, 8982−8986.
(11) Wang, Q.; Wong, C. F.; Rabitz, H. *Biophys. J.* **1998**, *75*, 60−69.
(12) Wendoloski, J.; Matthew, J. B. *Proteins* **1989**, *5*, 313−321.
(13) Laberge, M.; Vreugdenhil, A. J.; Vanderkooi, J. M.; Butler, I. S. *J. Biomolec. Struct. Dyn.* **1998**, *15*, 1039−1050.
(14) Zhou, H.; Vijayakumar, M. *J. Mol. Biol.* **1997**, *267*, 1002−1022.
(15) Zheng, C.; Wong, C. F.; McCammon, J. A. *Biopolymers* **1990**, *29*, 1877−1883.
(16) Laberge, M.; Köhler, M.; Vanderkooi, J. M.; Friedrich, J. *Biophys. J.* **1999**, *77*, 3293−3304.
(17) Crowe, L. M.; Reid, D. S.; Crowe, J. H. *Biophys. J.* **1996**, *71*, 2087−2093.
(18) Beece, D.; Eisenstein, L.; Frauenfelder, H.; Good, D.; Marden, M. C.; Reinisch, L.; Reynolds, A. H.; Sorensen, L. B.; Yue, K. T. *Biochemistry* **1980**, *19*, 5147−5157.
(19) Cordone, L.; Galajda, P.; Vitrano, E.; Gassmann, A.; Ostermann, A.; Parak, F. *Eur. Biophys. J.* **1998**, *27*, 173−176.
(20) Hagen, S. J.; Hofrichter, J.; Eaton, W. A. *Science* **1995**, 959−962.
(21) Green, J. L.; Angell, C. A. *J. Phys. Chem.* **1989**, *93*, 2880−2882.
(22) Branca, C.; Magazu, S.; Maisano, G.; Migliardo, P. *J. Phys. Chem. B* **1999**, *103*, 1347−1353.
(23) Magazu, S.; Maisano, G.; Migliardo, P.; Musolino, A. M.; Villari, V. *Philos. Mag. B* **1998**, *77*, 655−661.
(24) Douzou, P. *Cryobiochemistry. An Introduction*; Academic Press: London, 1977.
(25) Bushnell, G. W.; Louie, G. V.; Brayer, G. D. *J. Mol. Biol.* **1990**, *214*, 585−595.
(26) MacKerell, A. A., Jr.; Bashford, M.; Bellott, R. L.; Dunbrack, J. D., Jr.; Evanseck, J. J.; Field, S.; Fischer, S.; Gao, J.; Guo, H.; Ha, S.; Joseph-McCarthy, D.; Kuchnir, L.; Kuczera, K.; Lau, F. T. K.; Mattos, C.; Michnick, S.; Ngo, D. T.; Nguyen, D. B.; Prodhom, W. E.; Reiher, B., III; Roux, M.; Schlenkrich, J. C.; Smith, R.; Stote, J.; Straub, J.; Watanabe, J.; Wiorkiewicz-Kuczera, D.; Yin, D.; Karplus, M. *J. Phys. Chem. B* **1998**, *102*, 3586−3616.
(27) Brooks, B. R.; Bruccoleri, R. E.; Olafson, B. D.; States, D. J.; Swaminathan, S.; Karplus, M. *J. Comput. Chem.* **1983**, *4*, 187−217.
(28) Jorgensen, W. L.; Chandrasekhar, J.; Madura, J. D.; Impey, R. W.; Klein, M. L. *J. Chem. Phys.* **1983**, *79*, 926−935.
(29) Harris, D.; Loew, G. *J. Am. Chem. Soc.* **1993**, *115*, 5799−5802.
(30) Loew, G. H. *Int. J. Quantum Chem.* **2000**, *77*, 54−70.
(31) Sato, R.; Yoshihiro, T.; Era, M.; Kashiwagi, H. *Chem. Phys. Lett.* **2001**, *341*, 645−651.
(32) Librizzi, F.; Vitrano, E.; Cordone, L. *Biophys. J.* **1999**, *76*, 2727−2734.
(33) Jeffrey, G. A. *An Introduction to Hydrogen Bonding*; Oxford University Press: New York, 1997.
(34) Carpenter, J. F.; Crowe, J. H. *Biochemistry* **1989**, *28*, 3916−3922.
(35) Manas, E. S.; Getahun, Z.; Wright, W. W.; DeGrado, W. F.; Vanderkooi, J. M. *J. Am. Chem. Soc.* **2000**, *122*, 9883−9890.
(36) Garcia, A. E.; Hummer, G. *Proteins: Struct., Funct., Genet.* **1999**, *36*, 175−191.
(37) Prabhu, N. V.; Perkyns, J. S.; Pettitt, B. M. *J. Peptide Res.* **1999**, *54*, 394−407.
(38) Small, G. J. Persistent Nonphotochemical Hole Burning and the Dephasing of Impurity Electronic Transitions in Organic Glasses. In *Spectroscopy and Excitation Dynamics of Condensed Molecular Systems*; Agronovich ,V. M., Hochstrasser, R. M., Eds.; North-Holland: Amsterdam, 83; pp 515−554.
(39) Rebane, L. A.; Gorokhovskii, A. A.; Kikas, J. V. *Appl. Phys. B* **1982**, *29*, 235−250.
(40) Fox, K. C. *Science* **1995**, *267*, 1922−1923.
(41) Vegis, A. *Annu. Rev. Plant Physiol.* **1964**, *15*, 185−224.
(42) Magazu, S.; Maisano, G.; Migliardo, P.; Villari, V. *J. Chem. Phys.* **1999**, *111*, 9086−9092.
(43) Kaposi, A. D.; Fidy, J.; Manas, E. S.; Vanderkooi, J. M.; Wright, W. W. *Biochim. Biophys. Acta* **1999**, *1435*, 41−50.
(44) Gottfried, D. S.; Peterson, E. S.; Sheikh, A. G.; Wang, J.; Yang, M.; Friedman, J. M. *J. Phys. Chem.* **1996**, *100*, 12034−12042.
(45) Hagen, S. J.; Hofrichter, J.; Eaton, W. A. *J. Phys. Chem.* **1996**, *100*, 12008−12021.
(46) Sastry, G. M.; Agmon, N. *Biochemistry* **1997**, *36*, 7097−7108.
(47) Stavrov, S. S.; Wright, W. W.; Vanderkooi, J. M.; Fidy, J.; Kaposi, A. M. *Biophys. J.* **2001**, *81*, 3472−3482.
(48) Churg, A. K.; Warshel, A. *Structure and Motions: Membranes, Nucleic Acids and Proteins*; Academic Press: New York, 1985; pp 371−385.
(49) Langen, R.; Brayer, G. D.; Berghuis, A. M.; McLendon, G.; Sherman, F.; Warshel, A. J. *J. Mol. Biol.* **1992**, *224*, 589−600.
(50) Muegge, I.; Qi, P. S.; Wand, A. J.; Chu, Z. T.; Warshel, A. *J. Phys. Chem. B* **1997**, *101*, 825−836.
(51) Sharp, K. A. *Biophys. J.* **1998**, *73*, 1241−1250.
(52) Hobbs, J. D.; Shelnutt, J. A. *J. Protein Chem.* **1995**, *14*, 19−25.
(53) Jentzen, W.; Ma, J.-G.; Shelnutt, J. A. *Biophys. J.* **1998**, *74*, 753−763.
(54) Garcia, A. E.; Hummer, G. *Proteins* **2000**, *38*, 261−272.
(55) Warshel, A.; Chu, Z. T.; Parson, W. W. *Science* **1989**, *246*, 112−116.
(56) Warshel, A.; Chu, Z. T. *J. Phys. Chem. B* **2001**, *105*, 9857−9871.
(57) Rovira, C.; Schulze, B.; Eichinger, M.; Evanseck, J. D.; Parrinello, M. *Biophys. J.* **2001**, *1981*, 435−445.
(58) Schlichter, J.; Fritsch, K.-D.; Friedrich, J.; Vanderkooi, J. M. *J. Chem. Phys.* **1999**, *110*, 3229−3234.
(59) Shibata, Y.; Takahashi, H.; Kaneko, R.; Kurita, A.; Kushida, T. *Biochemistry* **1999**, *38*, 1802−1810.
(60) Sutherland, J. C.; Klein, M. P. *J. Chem. Phys.* **1972**, *51*, 76−86.
(61) Collins, D. W.; Champion, P. M.; Fitchen, D. B. *Chem. Phys. Lett.* **1976**, *40*, 416−419.
(62) Suisalu, A.; Mauring, K.; Kikas, J.; Herenyi, L.; Fidy, J. *Biophys. J.* **2001**, *80*, 498−504.
(63) Swartz, P. D.; Beck, B. W.; Ichiye, T. *Biophys. J.* **1996**, *71*, 2958−2969.
(64) Kaposi, A. D.; Wright, W. W.; Fidy, J.; Stavrov, S. S.; Vanderkooi, J. M.; Rasnik, I. *Biochemistry* **2001**, *40*, 3483−3491.

(65) Laberge, M.; Osvath, S.; Fidy, J. *Biochemistry* **2001**, *40*, 9226−9237.
(66) Cordone, L.; Cupane, A.; Leone, M.; Vitrano, E. *Biophys. Chem.* **1986**, *24*, 259−275.
(67) Schomacker, K. T.; Champion, P. M. *J. Chem. Phys.* **1986**, *84*, 5314−5325.
(68) Cottone, G.; Cordone, L.; Ciccotti, G. *Biophys. J.* **2001**, *80*, 931−938.
(69) Schweitzer-Stenner, R.; Bigman, D. *J. Phys. Chem. B* **2001**, *105*, 7064−7073.
(70) Kumble, R.; Rush, T. S., III; Blackwood, M. E., Jr.; Kozlowski, P. M.; Spiro, T. G. *J. Phys. Chem. B* **1998**, *102*, 7280−7286.